BATTELLE-NORTHWEST
RECEIVED
APR 22 1971
REFERENCE COPY
TECHNICAL INFO. SECTION

BNWL-SA- 3724

1 —

RECORD COPY

CRITICAL HEAT FLUX & TWO PHASE HYDRAULIC INVESTIGATION OF A 16-ROD SIMULATION OF A BWR FUEL ASSEMBLY*

A. M. Sutey
D. E. Fitzsimmons
W. L. Thorne
L. B. Torobin

*This work performed by Battelle-Northwest under contract to the Jersey Nuclear Company.

A. M. Sutey, D. E. Fitzsimmons, and W. L. Thorne** - Battelle-Northwest, Richland, Washington.
L. B. Torobin - Jersey Nuclear Company, Bellevue, Washington.

**W. L. Thorne is presently with WADCO Corp., Richland, Washington.

MASTER

DISTRIBUTION OF THIS DOCUMENT IS UNLIMITED
RWR

DISCLAIMER

This report was prepared as an account of work sponsored by an agency of the United States Government. Neither the United States Government nor any agency thereof, nor any of their employees, make any warranty, express or implied, or assumes any legal liability or responsibility for the accuracy, completeness, or usefulness of any information, apparatus, product, or process disclosed, or represents that its use would not infringe privately owned rights. Reference herein to any specific commercial product, process, or service by trade name, trademark, manufacturer, or otherwise does not necessarily constitute or imply its endorsement, recommendation, or favoring by the United States Government or any agency thereof. The views and opinions of authors expressed herein do not necessarily state or reflect those of the United States Government or any agency thereof.

DISCLAIMER

Portions of this document may be illegible in electronic image products. Images are produced from the best available original document.

CRITICAL HEAT FLUX AND TWO PHASE HYDRAULIC INVESTIGATION OF A 16 ROD SIMULATION OF A BWR FUEL ASSEMBLY

A.M. Sutey, D.E. Fitzsimmons, W.L. Thorne & L. B. Torobin

ABSTRACT

The combined effects of local power distribution and grid spacers on CHF were experimentally evaluated using an electrically heated 16 rod bundle simulation of a typical BWR fuel assembly. The single and two-phase hydraulic behavior of the test assembly was also evaluated. Data were obtained over a range of pressures (1000-1500 psia), mass velocities (0.5×10^6 - 2.0×10^6 lb/hr ft^2), and bundle-average exit qualities (0 - .40). CHF consistently occurred upstream of the last grid spacer indicating that the grid spacer improved coolant mixing downstream of it. CHF results compared well with other rod bundle CHF data available in the literature. Rod bundle two-phase pressure losses were accurately predicted via the COBRA code using the Homogeneous two-phase model in conjunction with empirically established single-phase hydraulic correlations for the bundle components.

INTRODUCTION

The successful design of fuel for a nuclear reactor requires knowledge of the thermal hydraulic behavior of the candidate fuel design. Specifically, information is required on the "critical heat flux" (CHF) and pressure drop behavior of the fuel. Much progress has been made in recent years in understanding the thermal hydraulic characteristics of boiling water reactor fuel assemblies. Nevertheless, the current state of the art is not sufficiently advanced to accurately predict the effects of local heat flux variations and

grid spacer designs on CHF and pressure drop. Local power distributions affect subchannel mass velocities and qualities, and as a result, significantly affect CHF, especially if the local peaking occurs in the proximity of a limiting subchannel. Grid spacers can either improve or lower the CHF, depending on the relative role of mixing and liquid film disturbance incorporated in the design of the spacers. In addition, spacers contribute significantly to the pressure losses of a fuel assembly. In this study the combined effects of local power distribution and grid spacers on CHF and pressure drop were evaluated using an electrically heated rod bundle simulation of a typical BWR fuel assembly. Experimental results were obtained over appropriate ranges of pressure, mass velocity and quality.

DESCRIPTION OF EXPERIMENTATION

Heated Bundle

This study used a uniform axial, electrically heated 16-rod bundle which included prototypic grid spacers and simulated the local power distribution of a BWR fuel assembly. The detailed power distribution of the 16-rod bundle as presented in Figure 1 was chosen not only to simulate rod bundle regions of maximum power and rod bundle regions of maximum local variation in power, but also to reproduce bundle average and subchannel mass velocities and qualities which occur within a typical BWR assembly. Subchannel calculations were performed using the COBRA Code[1] to help synthesize the local power distribution for the 16-rod CHF simulation and to verify the thermal hydraulic simulation of an actual BWR fuel assembly using the 16 rod bundle. Details of the analysis used to synthesize the local power distribution of the rod bundle are presented in Appendix I.

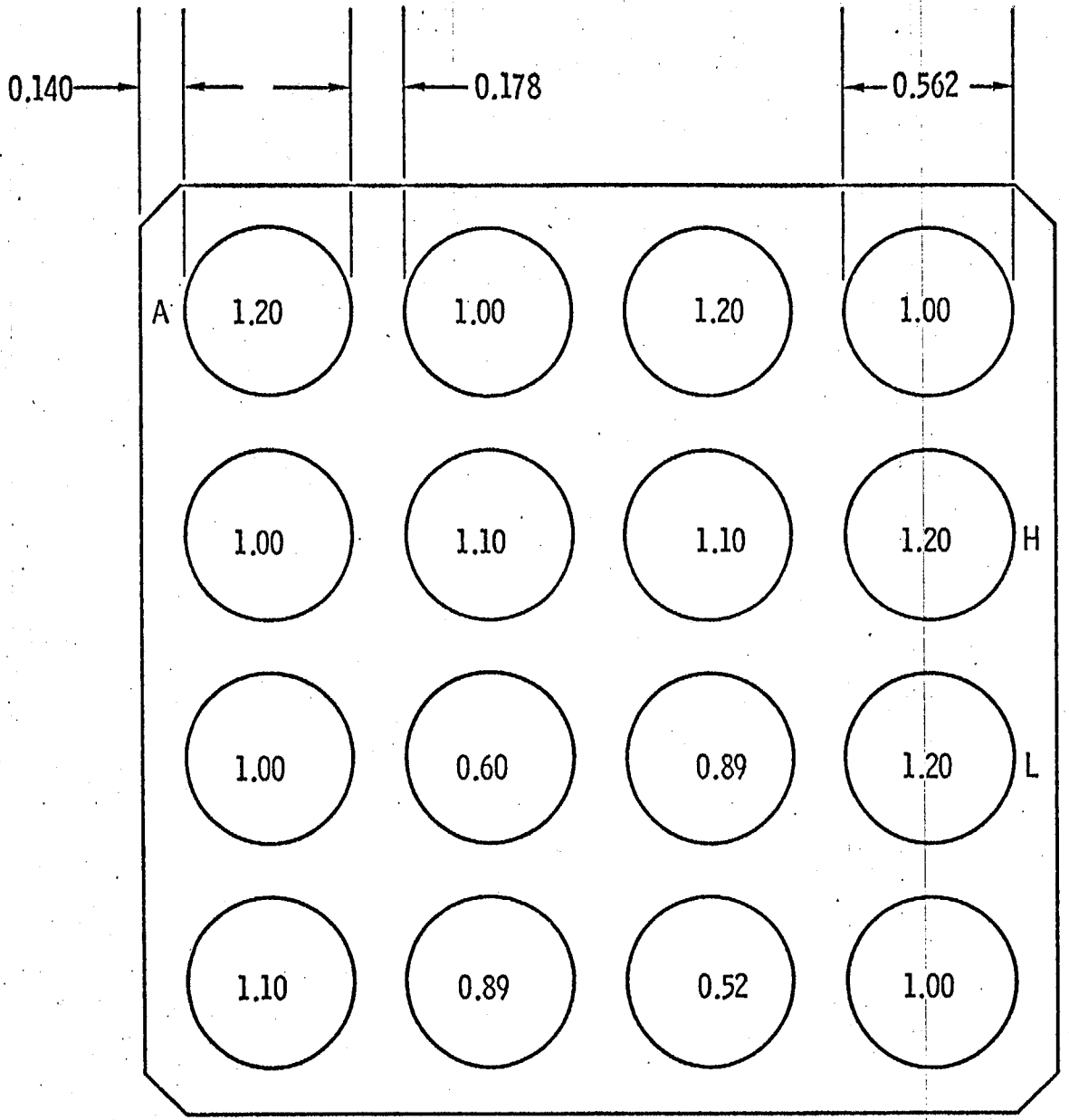

FIGURE 1. LOCAL POWER DISTRIBUTION OF CHF ASSEMBLY

A summary of the important geometric parameters of the rod bundle is presented in Table I. Schematic descriptions of the instrumented rod bundle and heater rods are presented in Figures 2 and 3. These figures also describe the locations of pressure and temperature monitors and grid spacer locations.

Each heater rod consisted of an Inconel-600 tube brazed at each end to copper connection rods of the same diameter as the tube. The wall thickness of each rod was selected to provide the proper relative heat flux when electrical current passed through it. Wall thicknesses ranged from 0.022 to 0.057 inches for the rods shown in Figure (1). The 16 heater rods were connected to electrical terminal plates at the inlet and outlet of the bundle via tapered mechanical joints at the ends of the copper connector rods. Both the inlet and outlet terminal plates were drilled to permit axial flow for the entire length of the bundle. The outlet tie plate was prototypic of an actual fuel assembly.

Heater rod temperature sensing and CHF detection was accomplished with thermocouples in conjunction with temperature sensing cylinders, which were inserted into each Inconel tube. A sheathed magnesium oxide insulated thermocouple was imbedded at the axis of each copper cylinder whose outside diameter was coated with a 0.005 in. ceramic glaze and which fit snugly within the heater tube. Each cylinder had 6 equally spaced radial grooves and a circumferential groove. In the case of a local hot spot anywhere around the tube circumference at one of these cylinder locations, the grooves directed the heat flow to the thermocouple. One 3/8 in. long cylinder was located at the downstream end of the heater tube; two 1 in. long cylinders

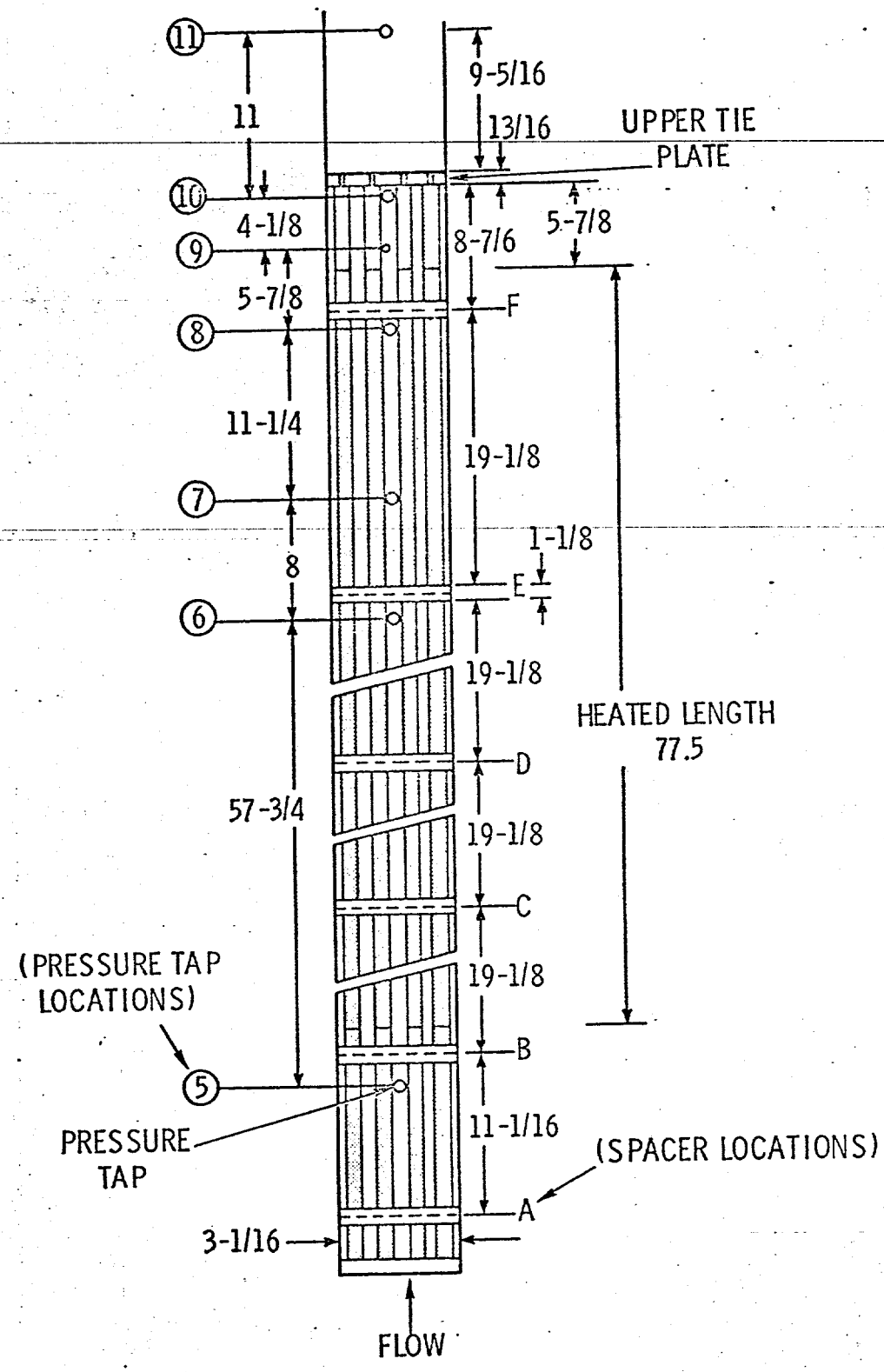

FIGURE 2. SCHEMATIC OF ROD BUNDLE TEST ASSEMBLY

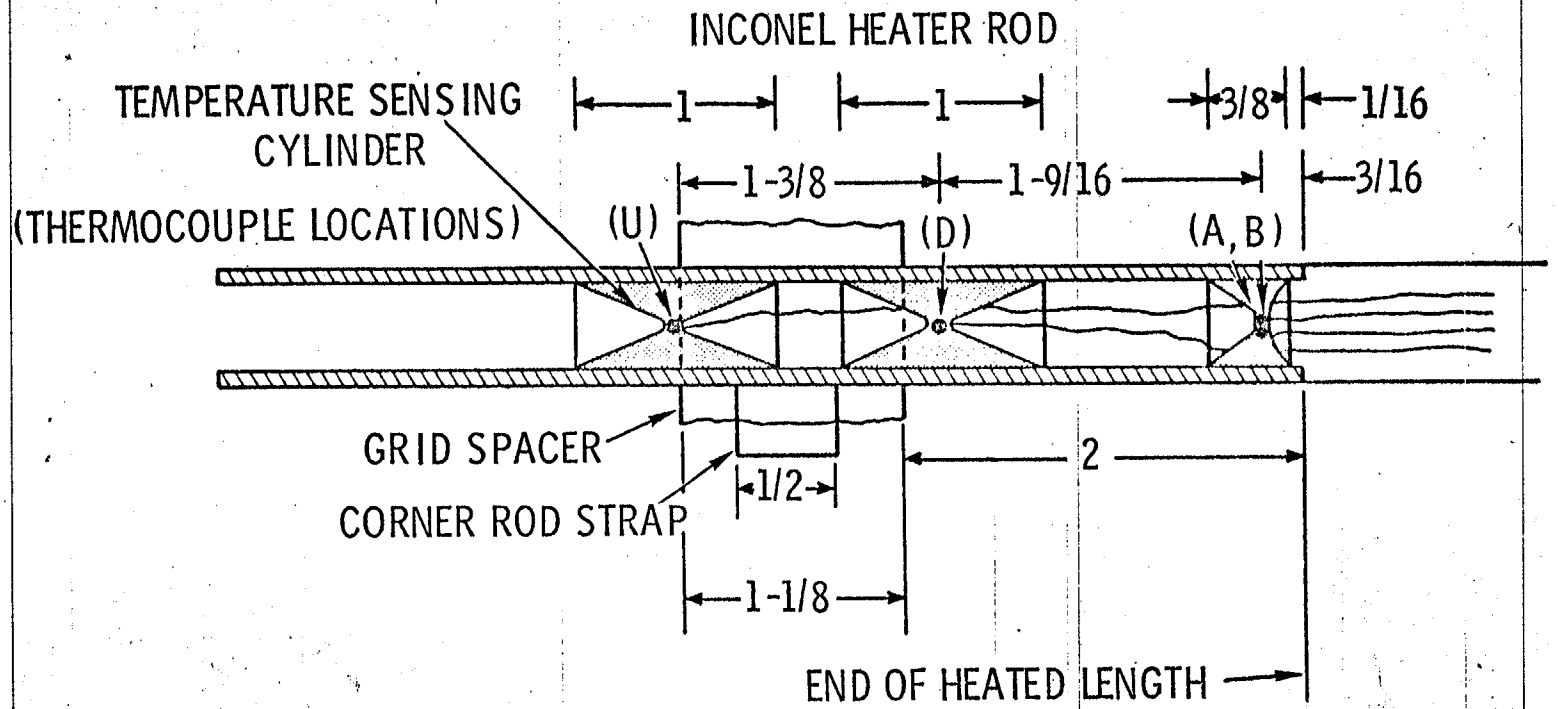

FIGURE 3. SCHEMATIC OF INSTRUMENTED HEATER ROD

were upstream on either side of the location of a prototype spacer whose flow disturbances might cause CHF.

A flow housing provided a square enclosure for the bundle and was enclosed in a pressure housing. The flow housing was electrically insulated from the rod bundle. As shown in Figure (2), pressure taps were provided along the length of the flow housing to define pressure losses across the rod bundle and its components. The taps were located at least 1 inch upstream or 6 inches (11 equivalent diameters) downstream of any restriction to ensure fully developed pressure readings.

In this study, typical BWR grid spacers were used. As shown in Figures (2) and (3), the top edge of the last grid spacer was located two inches upstream of the end of the heated length, and 19-1/8 in. downstream of the preceding grid spacer. This was an appropriate position to indicate whether the spacer accentuated or suppressed CHF downstream of itself. A minimum 10 mil thickness was removed from each grid spacer fuel rod support location and replaced with an equivalent amount of Rokide (Al_2O_3). In this manner, the grid spacers were electrically insulated from the electrically heated simulated fuel rods.

TABLE I. 16-ROD BUNDLE CHARACTERISTICS

Bundle Dimensions			
Rod diameter	0.562 in.	Equivalent diameter	0.531 in.
Rod pitch, square array	0.740 in.	Heated length	77.5 in.
Rod-rod spacing	0.178 in.	Heated area/pin	0.9502 ft^2
Square channel I.D.	3.062 in.	Heated area/bundle	15.204 ft^2
Rod-channel spacing	0.140 in.	Flow area	0.368 ft^2

Heat Transfer Facility

The experiments were performed in the vertical loop of the High Pressure Heat Transfer Facility at the Thermal Hydraulics Laboratory, Battelle-Northwest. This facility consists of a stainless steel flow loop which has a design rating of 2500 psig at 650°F and two large direct current power supplies. Fluid from a centrifugal pump rated at 250 gal/min and 1450 ft. head passed through an electrical preheater and then into the heated test assembly. Fluid from the test assembly passed into a large header, then through the condenser and returned to the pump suction.

The large direct current power supplies consist of 1) a silicon rectifier bank rated at 32,000 amperes at 125 volts (4.0 Megawatts) and 2) a motor-generator set rated at 25,000 amperes at 50 volts (1.25 Megawatts). The power to the rod bundle and to the preheater were supplied, respectively, by the rectifiers and the motor generators. The preheater was used primarily to provide two phase conditions at the test assembly inlet.

Test Procedure

Isotherms (Zero Rod Bundle Power)

Isothermal tests were performed prior to the CHF tests to provide data on heat losses, pressure losses and calibration of system instrumentation. Isothermal single phase pressure losses were experimentally obtained for the various components of the 16-rod CHF assembly over a range of mass velocities extending from 0.5 to 2.0 million lb/hr ft^2 and fluid temperatures ranging from 74 to 578°F. Precision differential manometers were used in this study to measure both single phase and two phase pressure losses.

Critical Heat Flux Runs

The power runs were performed by setting the pressure, flow, and coolant inlet enthalpy and by increasing the power to the test section in a series of steps. The size of the power steps varied, but at conditions near CHF the steps gave increases in the heat flux of 10,000 to 20,000 Btu/hr ft^2. After each power increase, the process variables were allowed to stabilize, and the data for the run recorded. The recorded data included two phase pressure losses for grid spacers, fuel rods, and the entire rod bundle.

The inception of CHF was determined from the wall temperatures of the heater rods. Prior to CHF, the temperatures increased by 5° to 15°F following each power increase. The onset of CHF was indicated by a rapid temperature rise of 25° to 100°F, or larger, on one or more rods during the power rise. The temperature generally leveled out, and the power was maintained until the data were recorded. CHF results of the 16-rod bundle were obtained over a range of pressures (1000-1500 psia), mass velocities (0.5-2.0 x 10^6 lb/hr ft^2), and bundle average exit quantities (0 - .40).

CRITICAL HEAT FLUX RESULTS

The CHF results are presented in Table II and in Figures 4 and 5 in the form of critical heat flux versus bundle average enthalpy and quality at the axial location of CHF. Critical heat flux occurred primarily on Rods A and H and to a limited extent on Rod L, all of which had peak to average flux ratios of 1.2. Consequently, for the power distribution of the rod bundle used in this study, the corner wall-subchannel surrounding Rod A and the wall subchannel surrounding Rod H were equally limiting from a CHF standpoint.

TABLE II.

Run No.	Press psia	Flow lb/hr ft^2 10^{-6}	Inlet Enthalpy Btu/lb	Heat Flux Btu/hr ft^2 10^{-6}	At CHF Location		Bundle Exit		CHF Location *	
					Enthalpy	Quality	Enthalpy	Quality	Rod	T/C
27	1165	0.5169	531	0.4205	799.2	0.375	810.4	0.393	A	U
29	1165	0.763	612.7	0.3754	774.8	0.336	781.7	0.347	A	U
34	1165	0.981	591.3	0.4159	731	0.265	736.9	0.275	A	U
40	1165	0.988	565.4	0.4678	721.8	0.25	728.4	0.261	A,H	U,U
46	1165	1.004	514	0.5356	690.3	0.199	697.7	0.211	H	U
55	1165	1.021	466	0.6349	671.5	0.169	680.1	0.183	A,H	U,U
61	1165	1.007	413	0.7165	648.1	0.131	658	0.147	H	U
67	1165	1.014	376	0.7804	630.3	0.1624	641	0.12	H	U
73	1165	0.514	382	0.5516	736.5	0.274	751.4	0.30	H	U
78	1165	0.514	309	0.6254	710	0.231	726.9	0.258	A	U
82	1165	0.5154	240	0.6872	679.5	0.182	697.9	0.2115	A	U
87	1165	0.508	167	0.764	663.7	0.156	684.6	0.190	H	U
90	1000	0.9968	450.5	0.6503	666.1	0.19	675.1	0.204	H	U
94	1165	1.485	454	0.7608	623.3	0.019	630.4	0.1025	H	U
98	1165	0.5075	454	0.4810	766.4	0.322	779.5	0.343	A	U**

* Rod and T/C (thermocouple) locations are presented in Figures 1 and 3, respectively.

** Slight indication on H-U

TABLE II. (Continued)

Run No.	Press psia	Flow lb/hr ft^2 10-6	Inlet Enthalpy Btu/lb	Heat Flux Btu/hr ft^2 10-6	At CHF Location		Bundle Exit		CHF Location*	
					Enthalpy	Quality	Enthalpy	Quality	Rod	T/C
104	1000	0.991	495	0.564	683.1	0.217	691	0.279	A,H	U,U
108	1000	0.994	554.9	0.4674	710.3	0.258	716.8	0.269	A	U
113	1165	1.536	493	0.682	639.8	0.118	645.8	0.127	A,H	U,U
116	1165	1.51	540	0.5640	663	0.155	669		A	U
120	1165	1.493	574	0.4679	677.3	0.178	681.7	0.185	A	U
124	1000	1.544	525	0.5870	650.3	0.166	655.5	0.174	A	U
128	1000	1.508	548.5	0.5292	664.1	0.187	669	0.195	A	U
133	1000	1.51	484	0.7061	638.5	0.148	645	0.158	A,H	U,U
137	1000	1.525	430	0.8138	606.3	0.098	613.7	0.1098	H	U
140	1500	1.003	392	0.7444	637.2	0.046	647.6	0.065	H	U
143	1500	0.9849	461	0.6358	674.3	0.113	683.3	0.1288	H,L	U,U
146	1500	0.9915	532	0.5067	700.4	0.16	707.5	0.1724	A	U
151	1500	1.001	600	0.380	725.5	0.205	730.8	0.214	A,H	U,U
154	1000	1 986	536	0.6227	639.3	0.1493	643.7	0.156	A	U
157	1000	2.006	515	0.6969	629.8	0.135	634.6	0.142	A,H	U,U
160	1000	1.972	486	0.7621	613.7	0.11	619	0.118	A,H	U,U
163	1000	2.028	466	0.8128	598.4	0.086	604	0.095	A,H	U,U
166	1000	1.516	462	0.7495	625	0.127	631.8	0.138	A	U
169	1500	1.002	425	0.680	649.4	0.068	658.8	0.085	H	U
172	1000	1.003	347	0.8412	624	0.126	635.7	0.1437	H,L	U,U

* Rod and T/C (thermocouple) locations are presented in Figures 1 and 3, respectively.

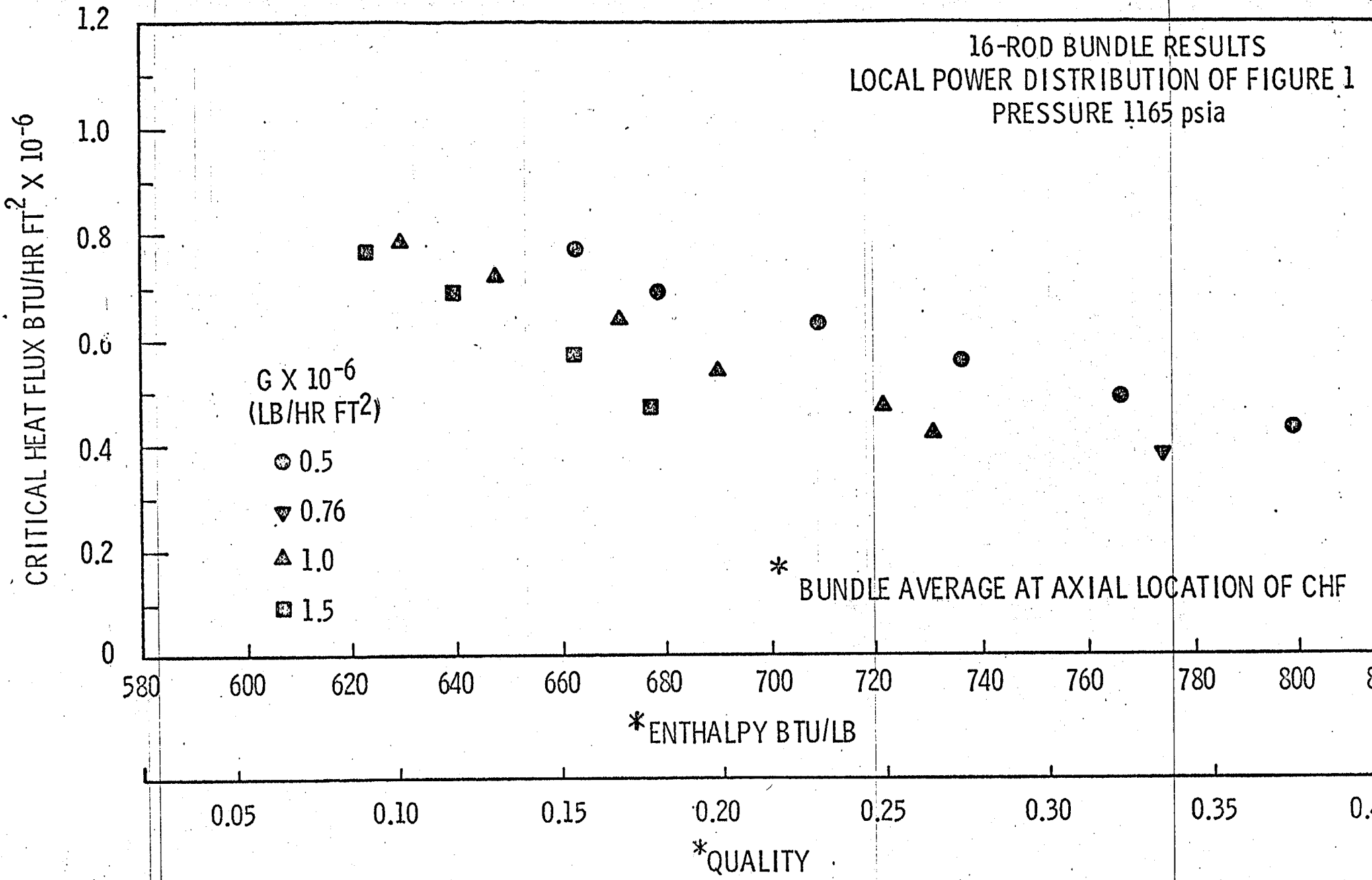

FIGURE 4. CRITICAL HEAT FLUX DATA AT PRESSURE OF 1165 psia

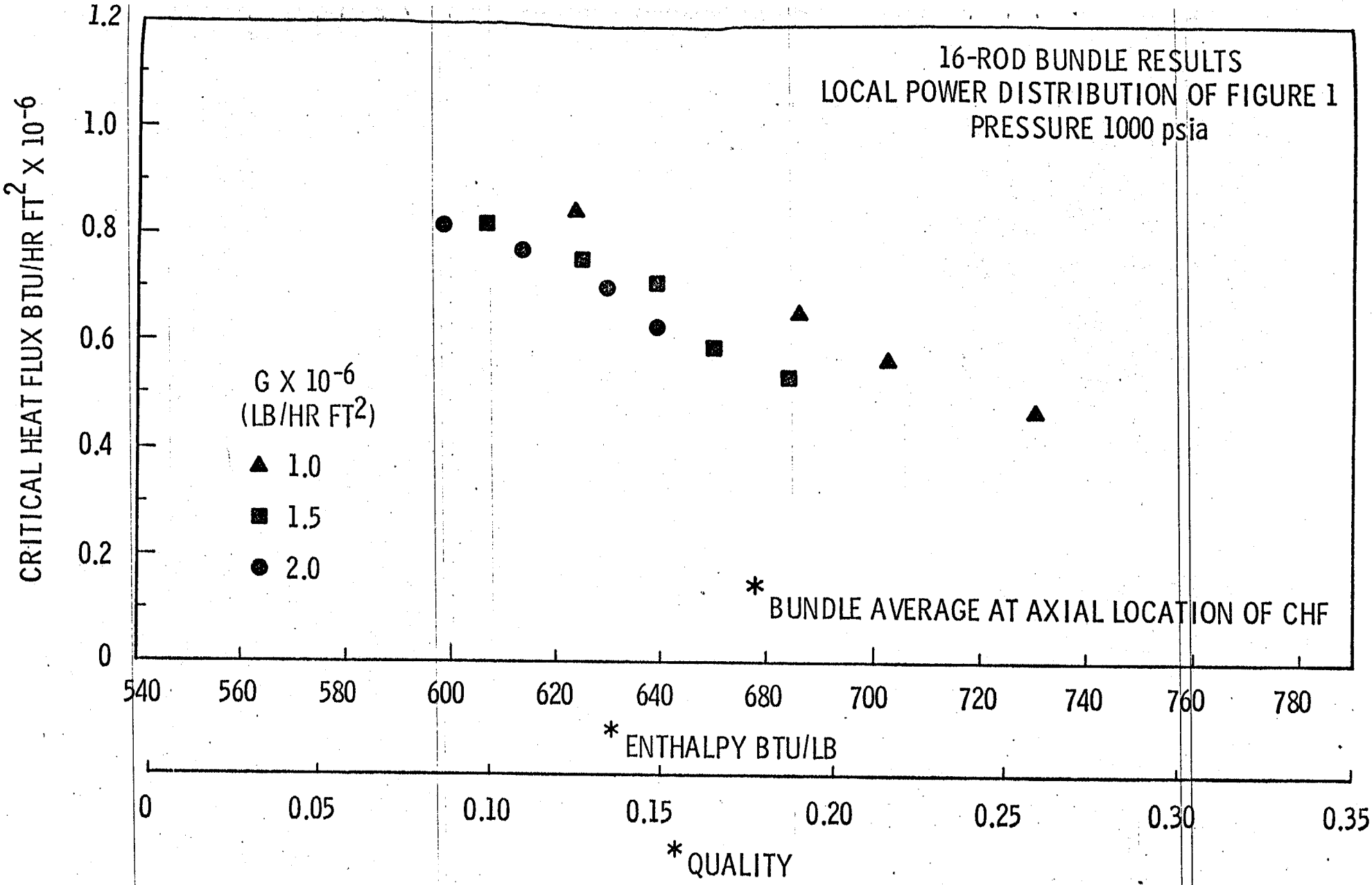

FIGURE 5. CRITICAL HEAT FLUX DATA AT REFERENCE PRESSURE OF 1000 psia

The top edge of last grid spacer was located two inches upstream of the end of the heated length. Surface temperatures were monitored slightly upstream and slightly downstream of the grid spacer and at the extreme end of the heated length. Visual observation of the test assembly subsequent to testing showed dry-out patterns upstream of the final grid spacer on Rods A, H, and L. In each case, these teardrop shaped patterns faced the unheated channel wall. For Rods H and L, the dryout patches began at the upstream edge of the grid spacer and extended upstream about one inch. In the case of the corner Rod A, the dryout patch began at the upstream edge of the spacer strap and extended upstream one to two inches.

The aforementioned results demonstrate that the grid spacer used in this study had no detrimental effect on CHF. In a uniform-axial heated bundle, CHF generally occurs at the end of the heated length where the axial bulk enthalpy (quality) is greatest. However, in this study CHF consistently occurred upstream of the last grid spacer. Local subchannel enthalpy and flow conditions upstream of the spacer were more limiting than those downstream even though the bundle average enthalpy at the CHF location was lower than that at the exit. Apparently, the spacer improved coolant mixing so that enthalpy and flow imbalances upstream of the grid spacer did not persist immediately downstream of it.

Effect of Mass Velocity

The effect of mass velocity on CHF is shown in Figures 4 and 5. In Figure 4, the CHF decreases with increased mass velocity over the studied mass velocity range 0.5 to 1.5 million lb/hr ft^2. In Figure 5, the CHF decreases, as the mass velocity increases from 1.0 to 2.0 million. At low

mass velocities near G = 0.5 million, annular film flow is the dominant flow regime for the studied quality range. As the mass velocity increases from G = 0.5 to 1.5 million, the annular film is stripped from the heated rod due to increased steam velocities, thus lowering the CHF. At mass velocities greater than 1.5 million, droplet entrainment and deposition phenomena compensate for the film stripping effects, and the CHF does not deteriorate as rapidly.

Effect of Pressure on CHF Results

In Figure 6, CHF results for a mass velocity of 1.0×10^6 are presented as a function of bundle average quality for pressures of 1000, 1165, and 1500 psia. Presentation of the CHF results in this form which is commonplace in the literature shows a substantial inverse pressure effect on CHF. However, presentation of the data in this way does not provide a proper evaluation of the effect of pressure on CHF. Since quality is a dependent thermodynamic function of pressure, the true effect of pressure on CHF is masked when presented on this basis. Instead, the CHF data should be plotted versus bundle average enthalpy as in Figure 7 to properly evaluate the effect of pressure on CHF. Note that Figure 7 is a presentation of the very same CHF data presented in Figure 6. Undoubtedly, enthalpy is a more universal reference for CHF results. It can be concluded that CHF results obtained in this study over the range of pressures 1000 to 1500 psia are independent of pressure when correlated as a function of enthalpy.

To demonstrate further that the effect of pressure on CHF should be evaluated on an enthalpy basis, identical CHF results of Janssen et al[2] are presented versus quality and enthalpy in Figures 8 and 9, respectively. Comparison of points A and B in Figures 8 and 9 demonstrates how quality accentuates the effect of pressure on CHF. Notice that CHF results are

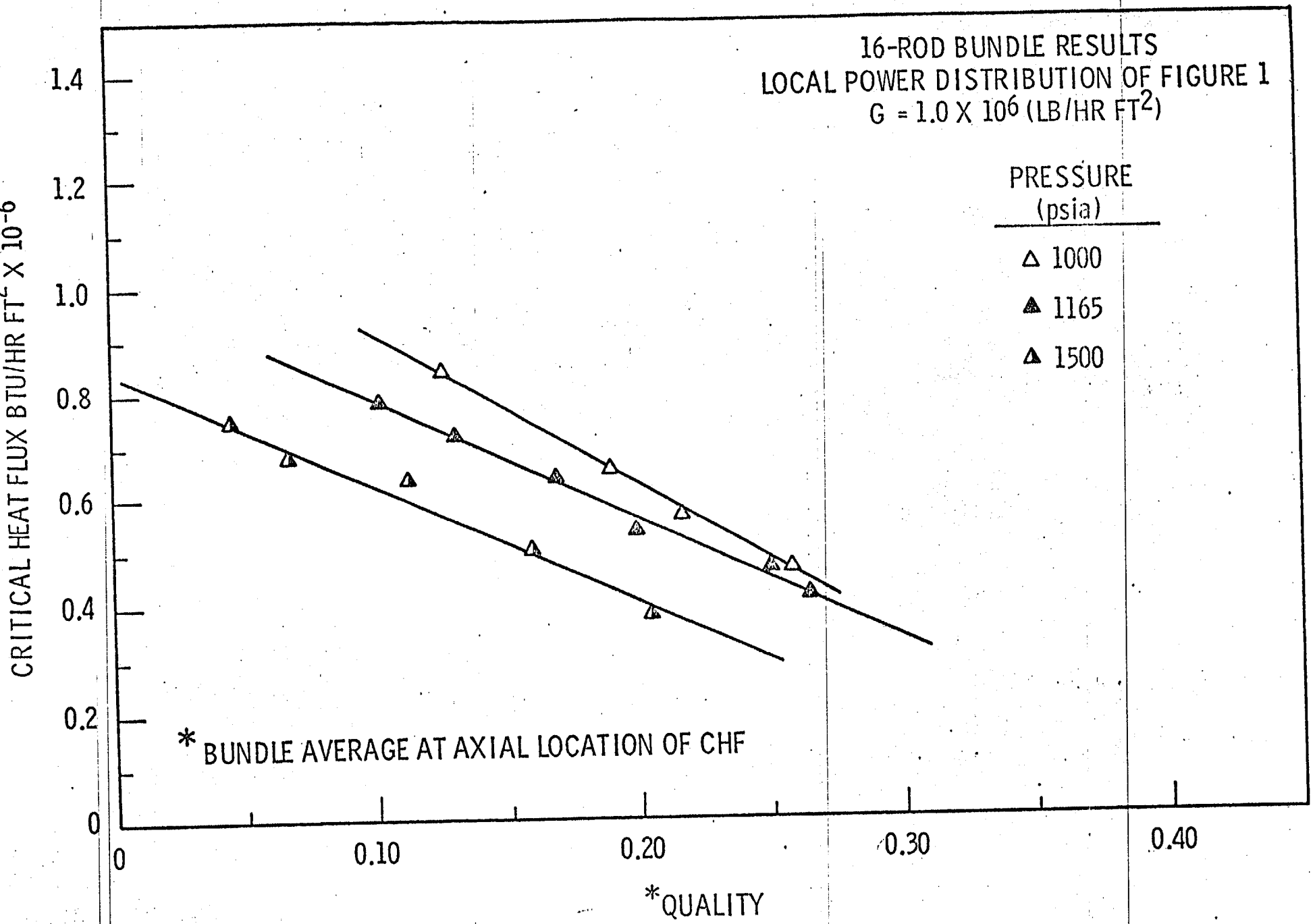

FIGURE 6. EFFECT OF PRESSURE - CRITICAL HEAT FLUX VS QUALITY

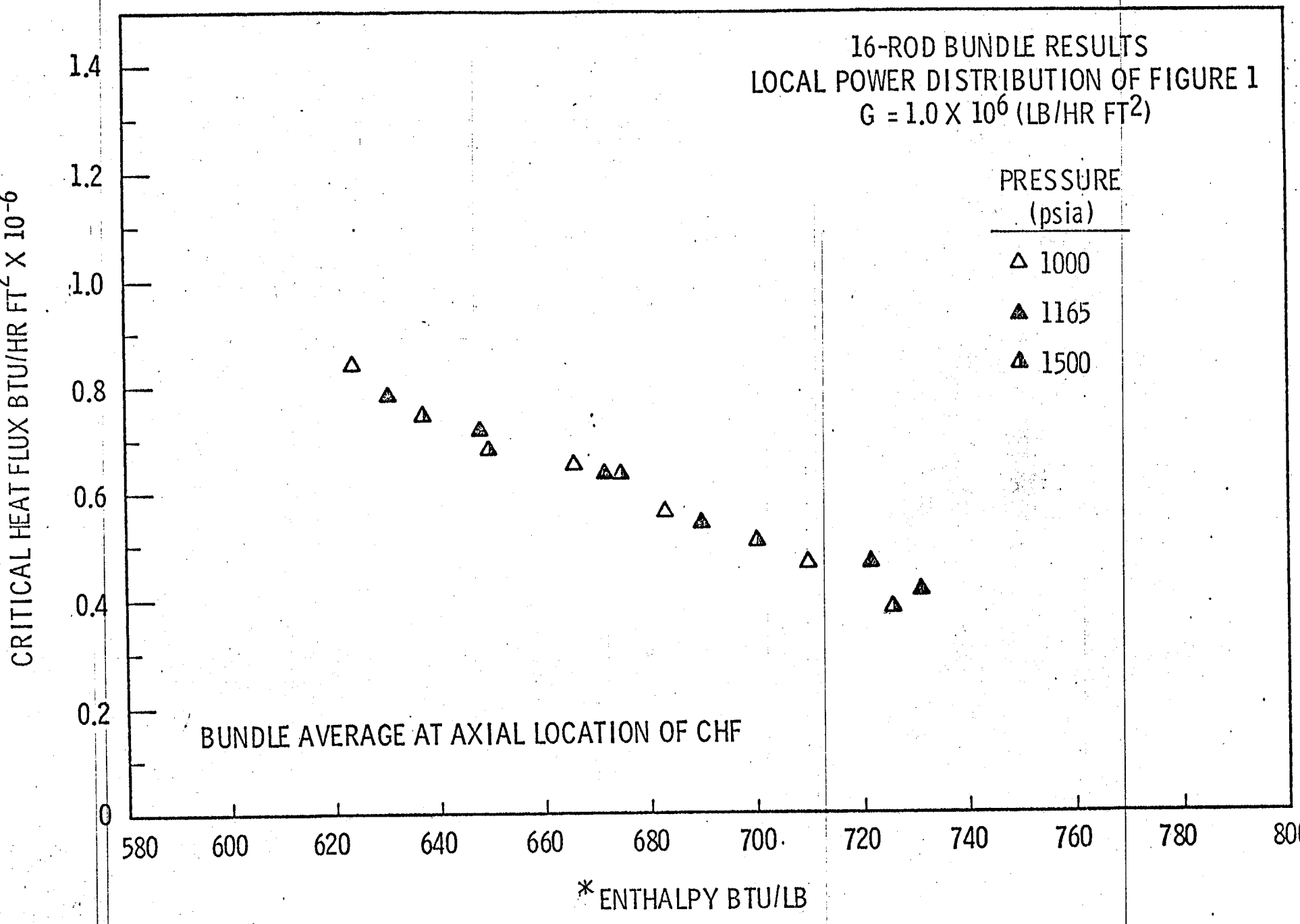

FIGURE 5. EFFECT OF PRESSURE - CRITICAL HEAT FLUX VS ENTHALPY

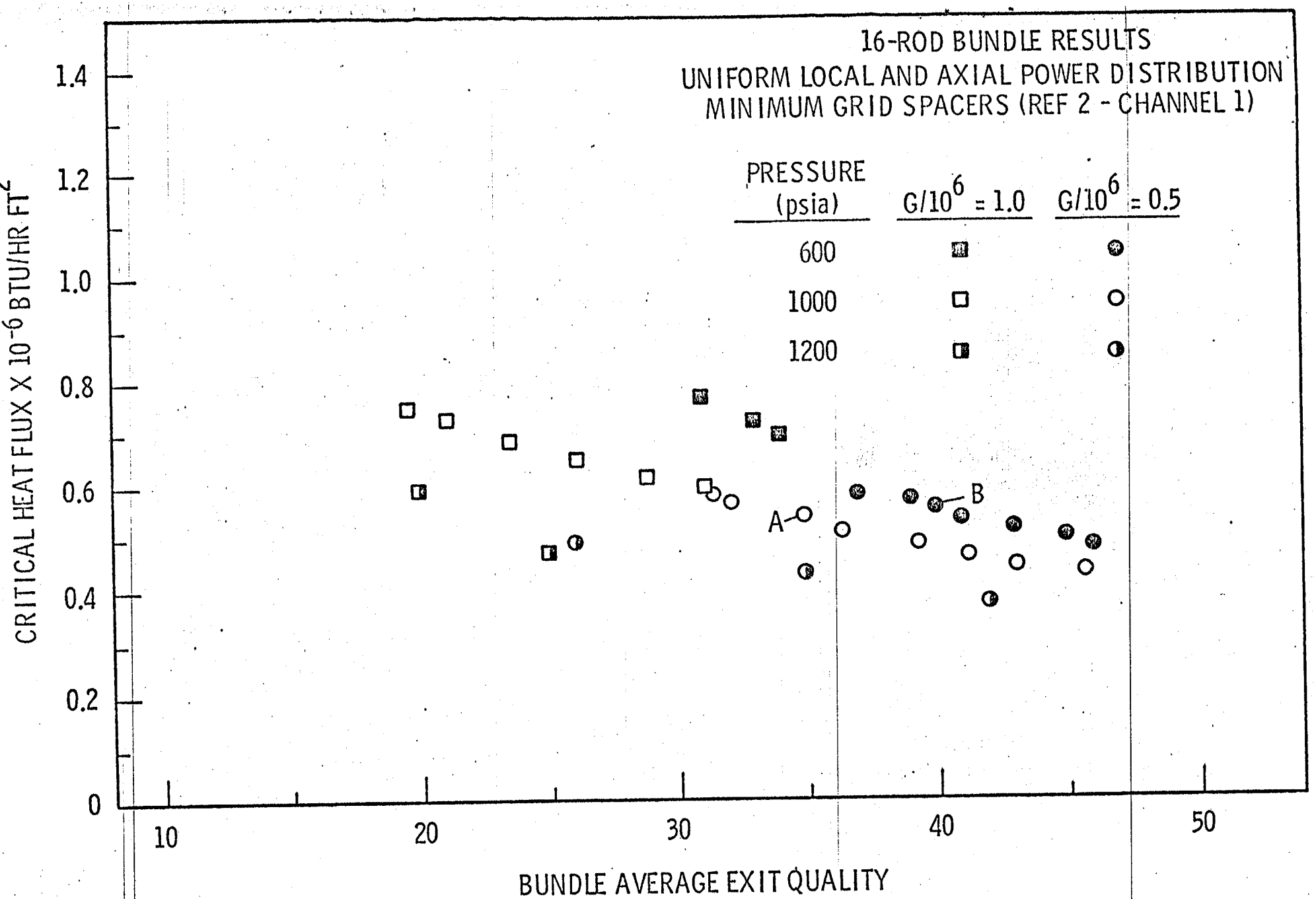

FIGURE 8. EFFECT OF PRESSURE - CRITICAL HEAT FLUX VS QUALITY

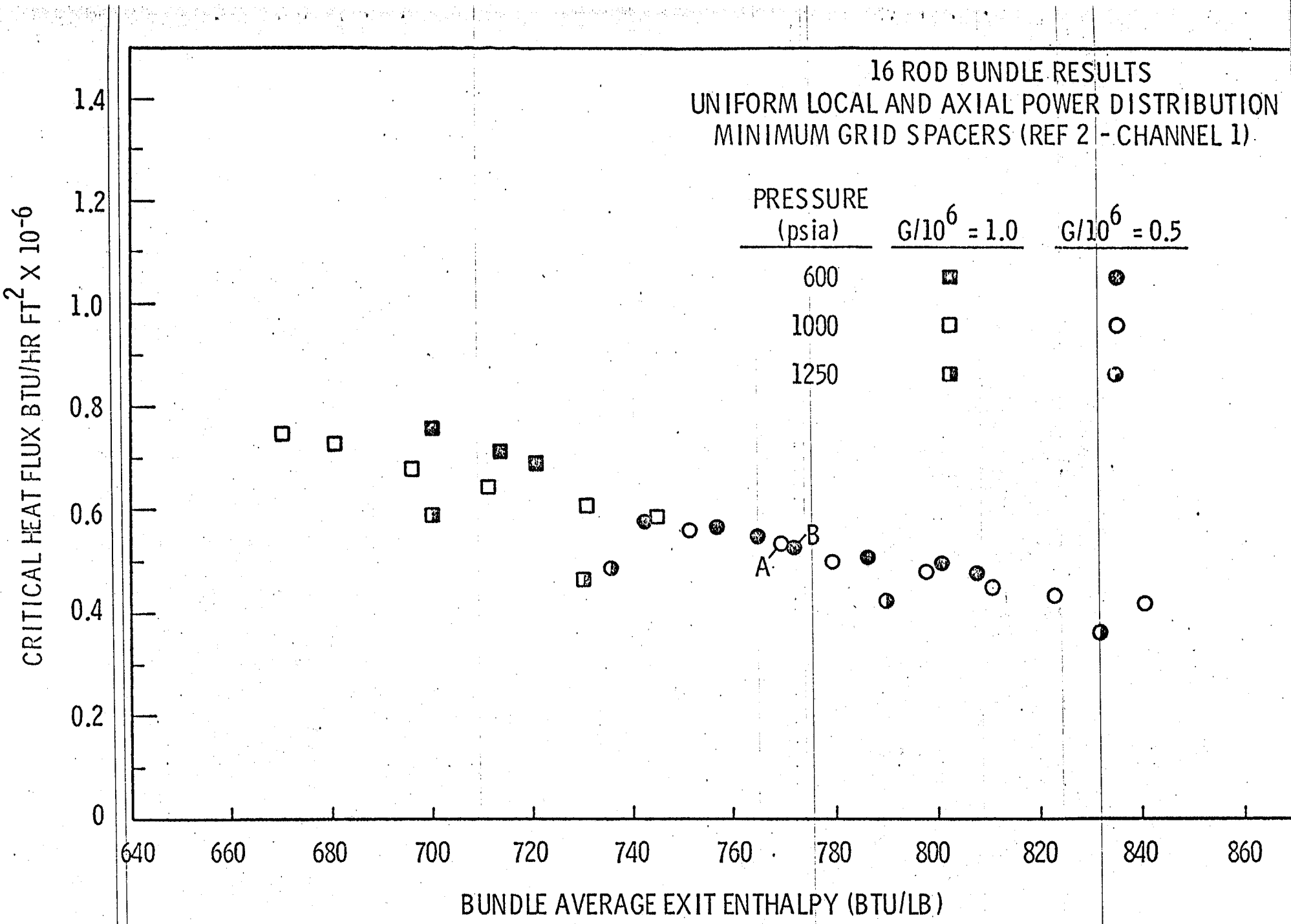

FIGURE 9. EFFECT OF PRESSURE - CRITICAL HEAT FLUX VS ENTHALPY

correlated much better on the enthalpy basis. Using the enthalpy basis, CHF results presented in Figure 9 still show a small pressure effect between 1000 to 1250 psia, whereas the results of this study show no substantial pressure effect between 1000 to 1500. These differences may well be explained by experimental error.

Comparison With Other CHF Data

It is desirable to compare the CHF results of the present study with data presented in the literature. Such a comparison is admittedly limited in value because of the differences in spacing, grid spacers and power distributions. In Figure 10, CHF results obtained in this study are compared with results of Janssen[2] for uniform axial and uniform local power distributions with and without grid spacers. The local power distribution affects subchannel mass velocities and qualities, and consequently, significantly affects the CHF especially if the peaking is in the proximity of a limiting subchannel. Figure 10 shows that for the same bundle average enthalpy the CHF for a bundle with local peaking in a limiting subchannel is less than that for a bundle with no local peaking.

In Figure 11, CHF results obtained in this study are compared with 16-rod bundle results of Israel et al[3] obtained with local power distributions with and without grid spacers. Several local power distributions were used in the test bundles; however, the corner rod had a 1.32 peak to average flux in all cases. On a bundle average enthalpy basis, the results of this study compare well with the results of Israel et al. Because of the differences in power distributions and spacers, the previous limited observation can only be made.

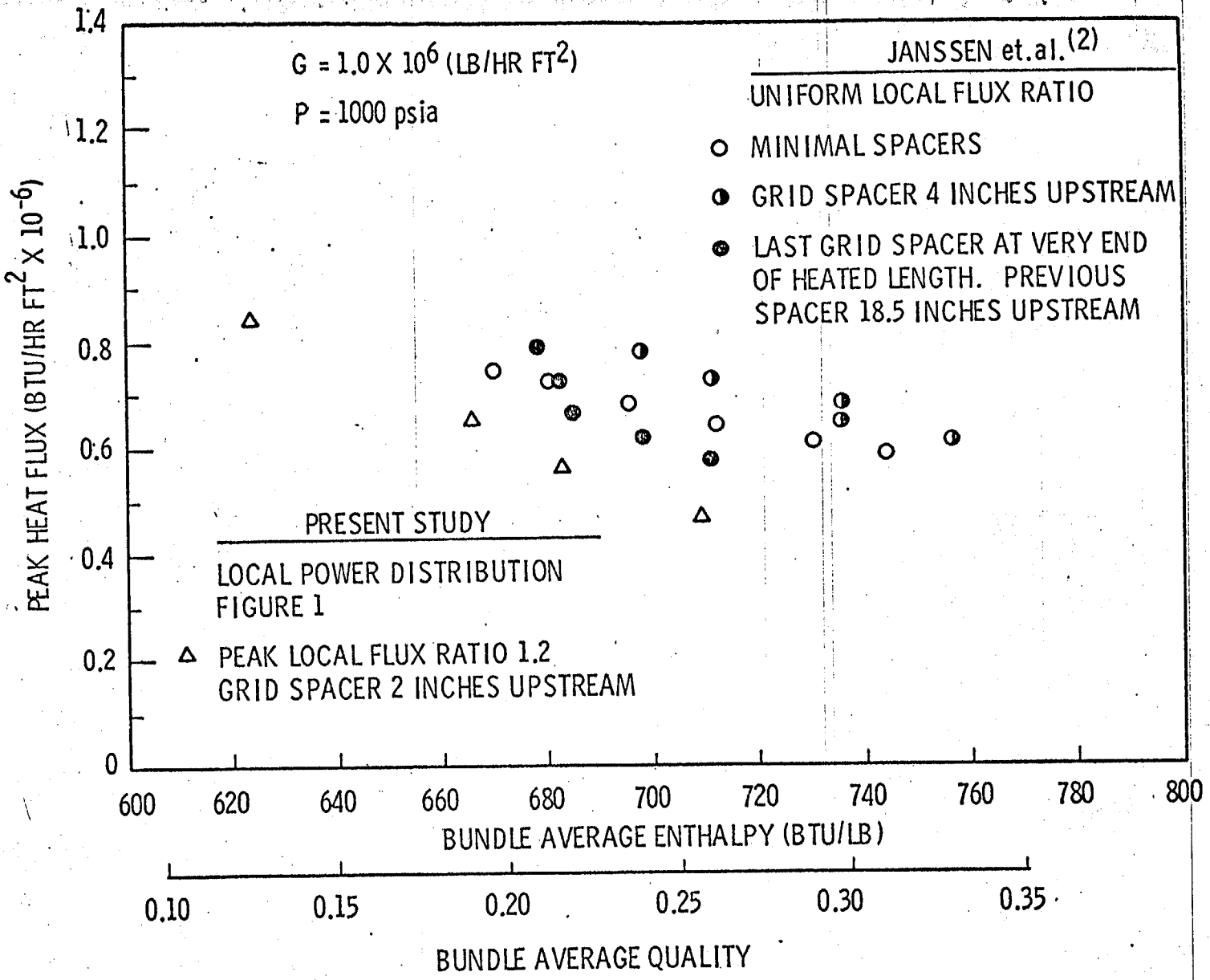

FIGURE 10. EFFECTS OF LOCAL POWER DISTRIBUTION ON BWR CHF RESULTS

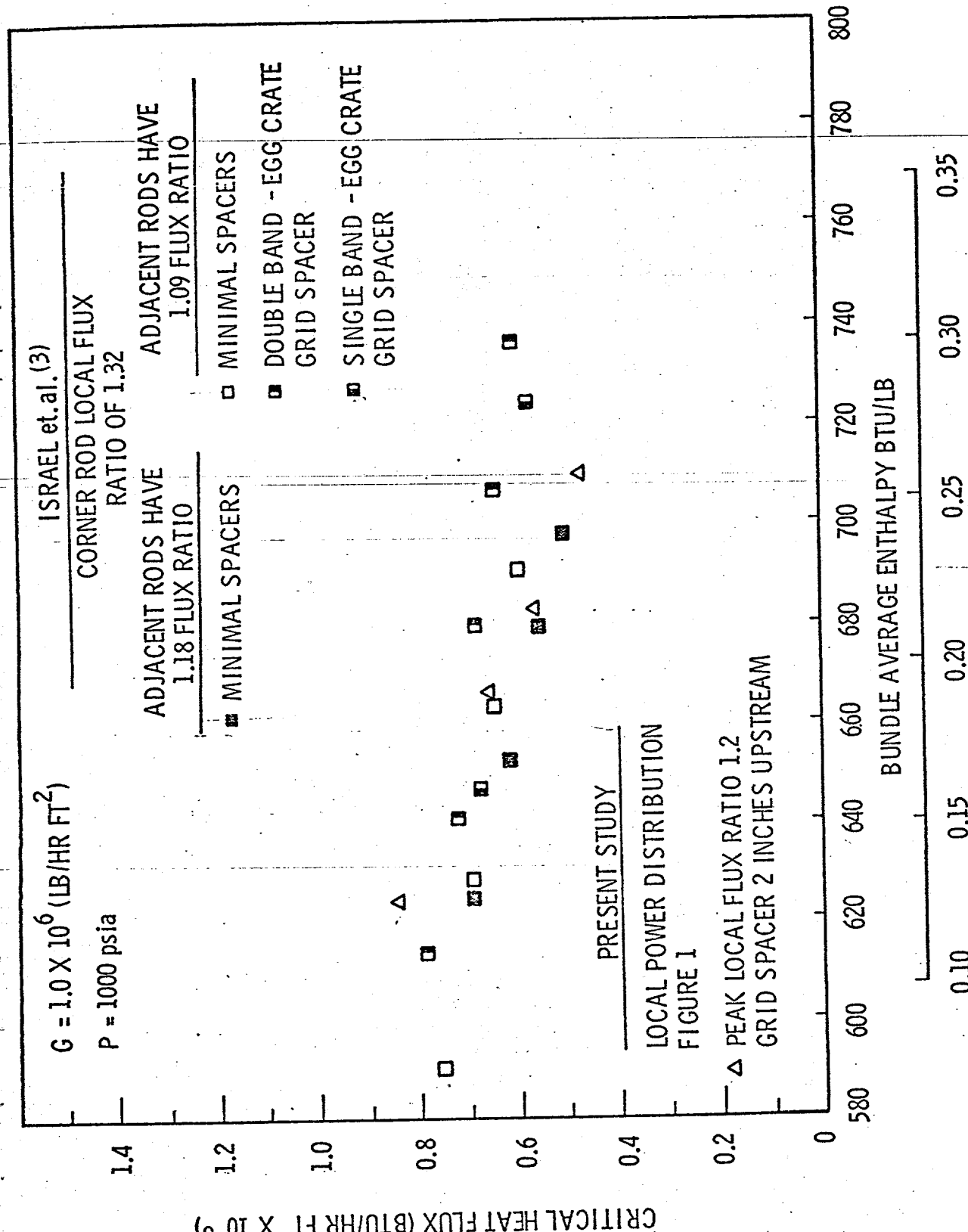

FIGURE 11. COMPARISON OF BWR CRITICAL HEAT FLUX DATA

Results of this study are also compared with the 16-rod bundle CHF results of Sofer and Soodak[4] in Figure 12. In their study, CHF results were obtained for a given local power distribution in which the peak to average flux ratio was varied. They used UNC grid spacers. As shown in Figure 12, CHF results obtained by Sofer and Soodak using a peak flux ratio of 1.23 compare very well on a bundle average basis with results of this study which used a 1.20 peak flux ratio.

In summary, it can be concluded that the CHF results of the present study compare well with the results of previous studies. However, additional insight concerning the effects of local power distributions and grid spacers on CHF can only be obtained by comparing the CHF results on a local sub-channel basis using a model such as COBRA[1]. Additional effort is required in this area.

HYDRAULIC RESULTS

Single Phase Isothermal Pressure Drop Results

Isothermal single phase pressure losses were obtained to establish that the essential hydraulic aspects of a typical BWR fuel assembly were properly simulated by the 16-rod bundle and to provide accurate single phase hydraulic information required for two phase pressure loss calculations.

Bare Rod Bundle

Friction factors for the bare rod bundle are presented in Figure 13. Over the Reynolds number range of 10,000 to 300,000, the experimental results can be fitted to a linear approximation $f = 0.256\ Re^{-0.206}$ where f is defined by $\Delta P = \frac{\rho f L V^2 BR}{d_e g_c}$

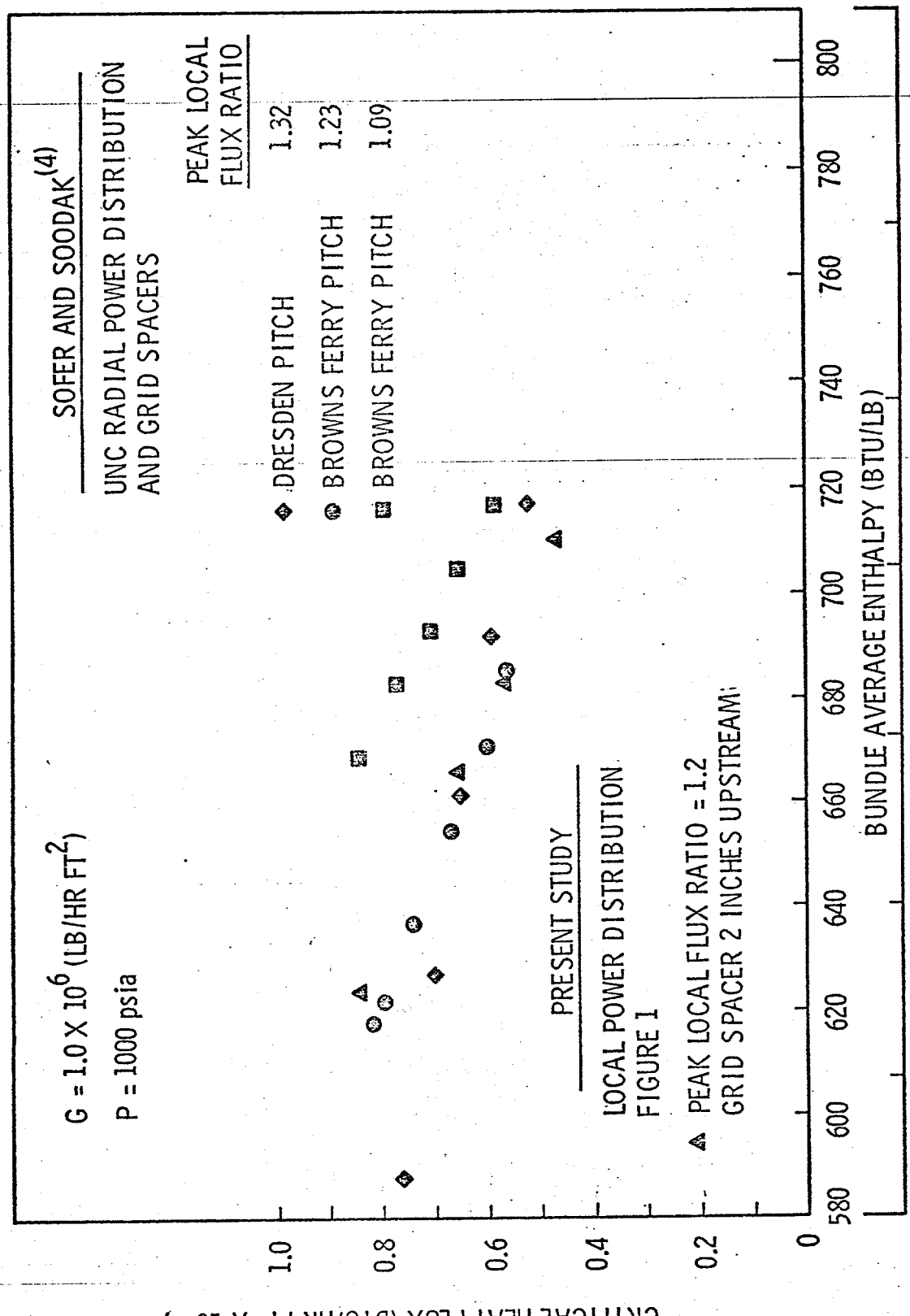

FIGURE 10. COMPARISON OF BWR CRITICAL HEAT FLUX DATA

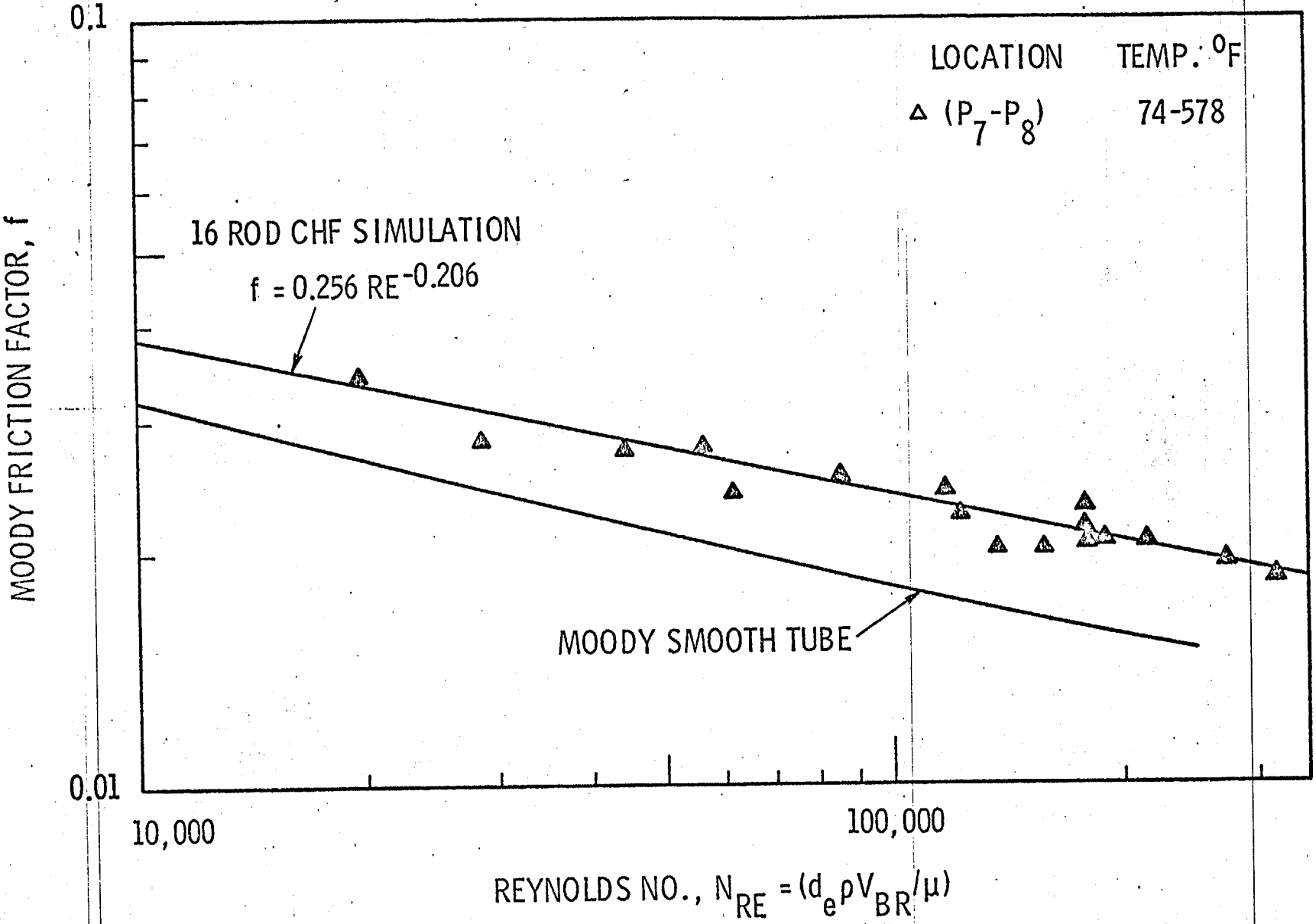

FIGURE 13. BARE ROD BUNDLE FRICTION FACTOR VS REYNOLDS NUMBER

Friction factors of the rod bundle are 25% higher than those of the Moody smooth tube prediction. This can be attributed to surface roughness of the rod bundle and to undeveloped boundary layers due to the presence of grid spacers in the rod bundle.

Grid Spacers

In Figure 14 pressure loss coefficients for two identical grid spacers are presented versus Reynolds number. The 4x4 grid spacers were good hydraulic simulations of typical BWR grid spacers to ensure proper simulation of CHF conditions in the CHF bundle. Results presented in Figure 14 show that the grid spacer pressure loss coefficients were independent of Reynolds number for Reynolds numbers greater than 300,000. For the 4x4 grid spacer $K = 4858\ Re^{-0.96} + 0.843$, where K is defined by the relation $\Delta P = -K\rho V^2_{BR}/2g_c$. These results compare very well with those reported by Grillo and Marinelli[5] and are presented in Figure 14 for comparison. On the basis of these results, a value of 0.9 may be used as a first approximation for preliminary analytical calculations involving typical BWR grid spacers for which accurate values of K are unavailable.

TWO PHASE PRESSURE DROP RESULTS

Two phase pressure drop-flow data were determined over appropriate ranges of mass velocity and bundle average exit quality at a constant system pressure typical of BWR operations. Experimental total pressure losses for the rod bundle extending from the beginning of the heated length to the exit of the upper tie plate are presented in Figure 15 and 16 as a function of bundle average exit quality at 1165 psia and for mass velocities of 0.52

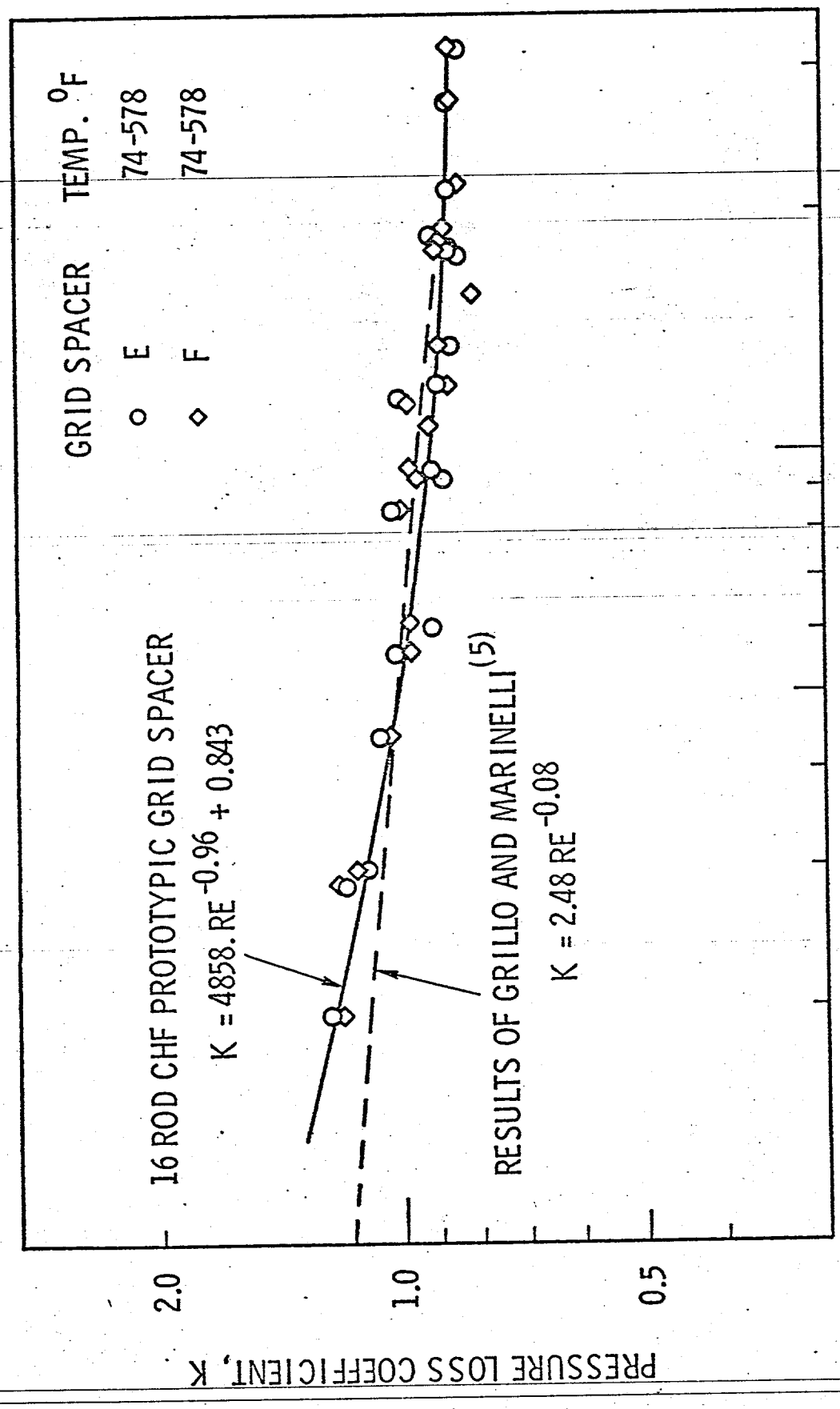

FIGURE 14. SPACER DRAG COEFFICIENT VS REYNOLDS NUMBER

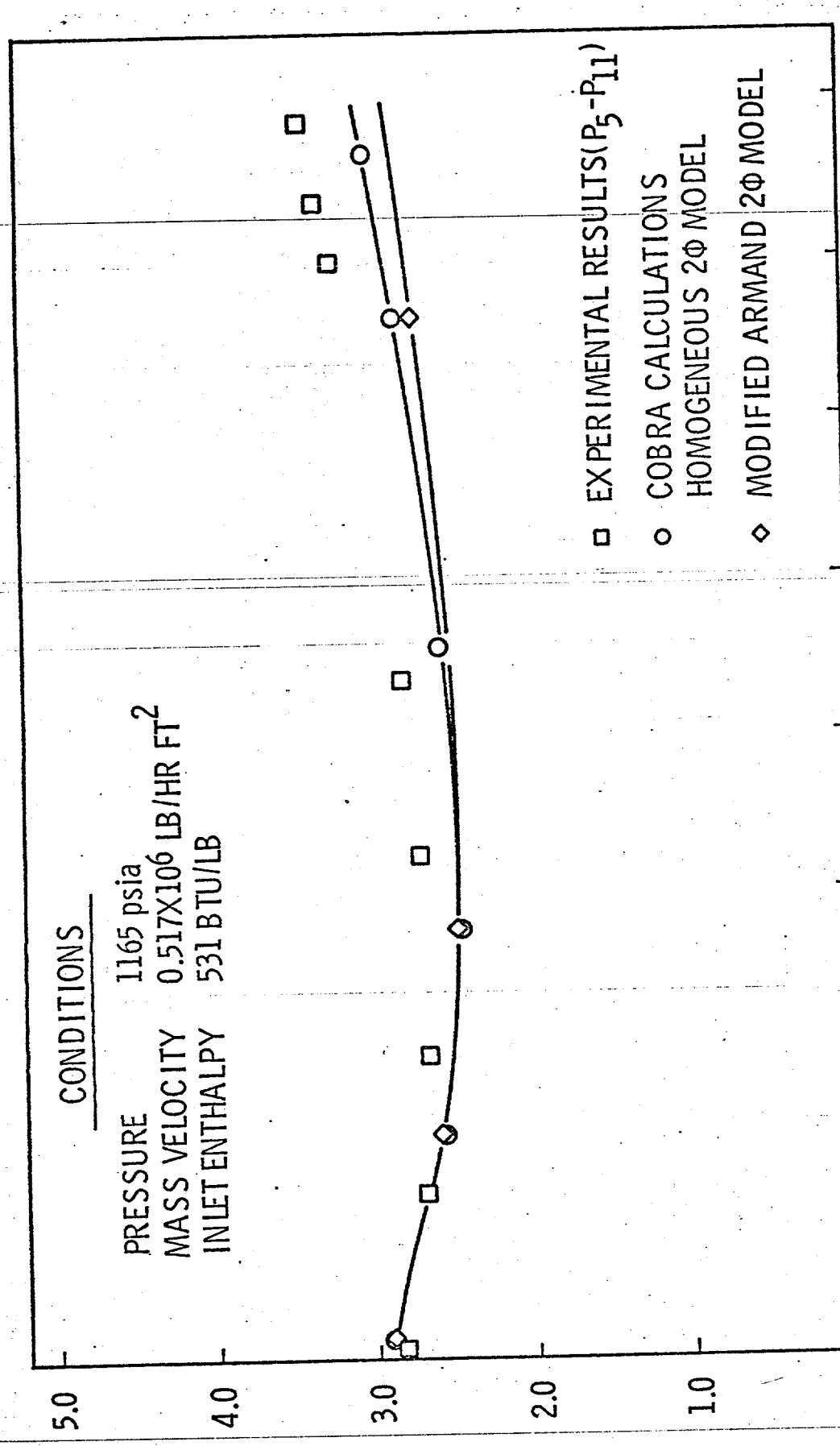

FIGURE 15: TWO PHASE PRESSURE LOSSES FOR 16 ROD BUNDLE.
$G = 0.5 \times 10^6$ LB/HR FT^2

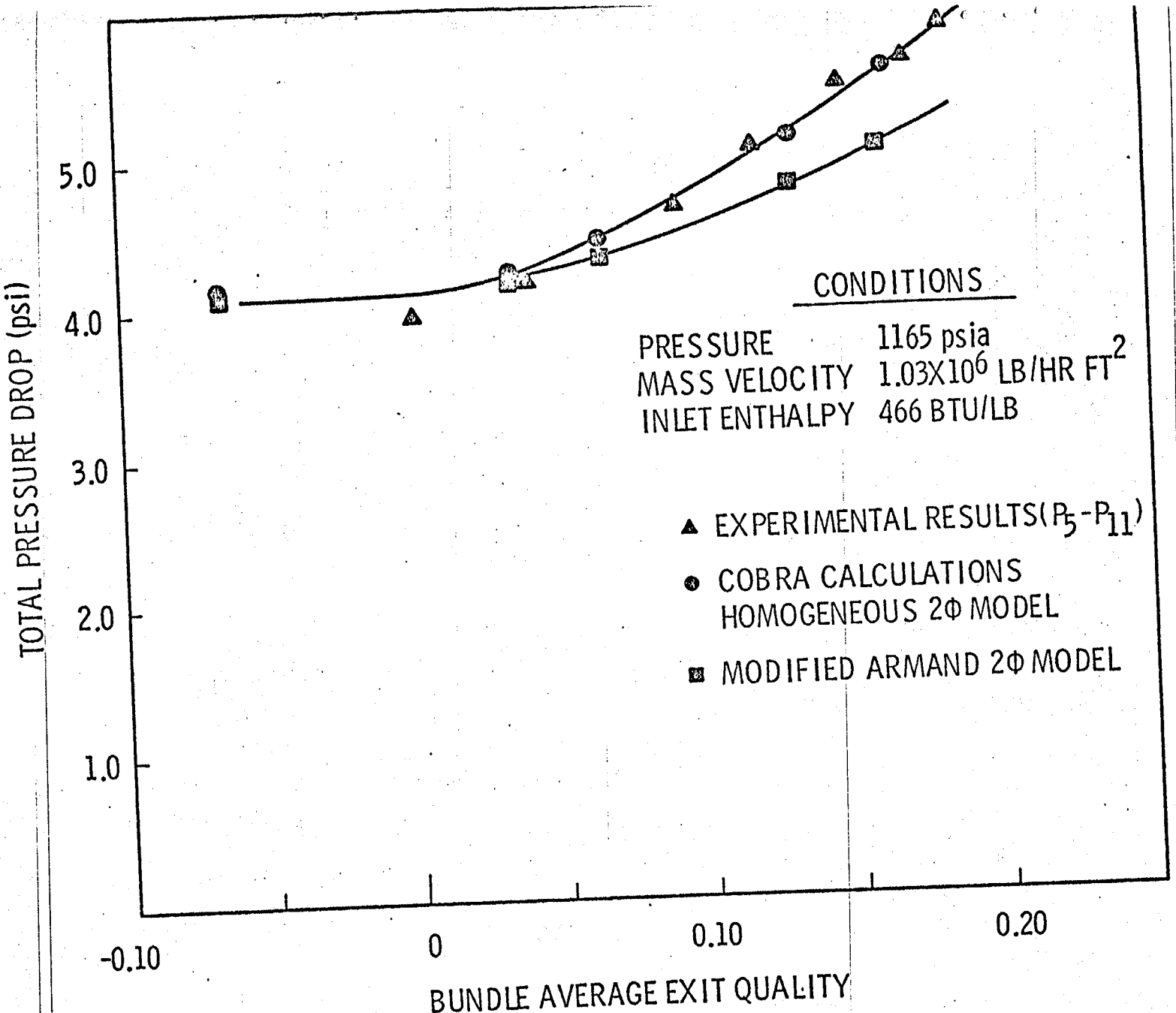

FIGURE 16. TWO PHASE PRESSURE LOSSES FOR 16 ROD BUNDLE
$G = 1.0X10^6$ LB/HR FT^2

and 1.03 million lb/hr ft^2, respectively. At a mass velocity of 0.52 lb/hr ft^2, the effect of quality on total pressure drop is not very great as shown in Figure 15. As the quality increases, friction and acceleration contributions to two phase pressure drop are balanced by decreasing gravitation pressure losses. However, at a mass velocity of 1.03 million lb/hr ft^2, two phase friction and acceleration pressure losses are dominant and the effect of quality on the total pressure loss is substantial as shown in Figure 16.

The COBRA[1] code was programmed to model the thermal-hydraulic behavior of the 16-rod bundle. Two phase friction losses for the fuel rods were predicted by applying two phase friction multipliers to the single phase friction factors experimentally establsihed for the rod bundle. Two-phase form and friction losses of the grid spacers were predicted using homogeneous two-phase mixture specific volumes and the experimentally established single phase grid spacer loss coefficients. COBRA calculations were performed using the Homogeneous and Modified Armand void fraction and two-phase friction multiplier models. Figures 15 and 16 show that the Homogeneous model predicts the experimental results better than does the Modified Armand Model. Most available void fraction and two-phase friction models are based on round tube rather than rod bundle data. Until rod bundle two-phase void fraction and friction multiplier models are developed, the Homogeneous model is recommended to predict two phase pressure losses.

As shown in Figures 15 and 16, COBRA two-phase pressure drop predictions compare well with the experimental results. COBRA two-phase pressure drop

predictions using the Homogeneous model are within 8% and 3% of the experimental results for mass velocities of 0.52 and 1.03 million lb/hr ft^2, respectively. Thus, COBRA can predict flow rates for the 4x4 rod bundle within 1.5 to 4.0%. These results indicate that rod bundle two-phase pressure losses can be accurately established via the COBRA code using the Homogeneous two-phase model in conjunction with empirically established single-phase correlations for the bundle components.

Conclusions

The grid spacer used in this study had no detrimental effect on CHF. In all cases CHF occurred upstream of the grid spacer even though bundle average enthalpy at the CHF location was lower than at the exit. The spacer improved coolant mixing so that enthalpy and flow imbalances upstream of the spacer did not persist downstream of it.

As the mass velocity increased from 0.5 to 2.0 million, the CHF decreased; however, at mass velocities greater than 1.5 million, the CHF does not deteriorate as rapidly.

CHF results obtained in this study over the range of pressure 1000 to 1500 psia are independent of pressure when correlated as a function of enthalpy.

For the same bundle average enthalpy, the CHF for a bundle with local peaking in a limiting subchannel is less than that for a bundle with no local peaking.

On a bundle average basis, the results of this study compare well with comparable results in the literature.

Single phase bare rod friction factors were approximately 25% higher than the Moody smooth tube values. This can be attributed to surface roughness of the rod bundle and to undeveloped boundary layers due to the presence of grid spacers in the rod bundle.

Single phase grid spacer pressure loss coefficients were independent of Reynolds number for Reynolds numbers greater than 300,000. Values of K for the grid spacer were close to 0.9.

Two phase rod bundle pressure losses can be accurately established via the COBRA code using the Homogeneous two-phase model in conjunction with empirically established single phase correlations for the bundle components.

APPENDIX I

Simulation of Local Power Distribution

A synthesized BWR local power distribution was used in this 16-rod bundle CHF simulation. Subchannel calculations were performed using the COBRA Code[1] to help synthesize the radial power distribution of the 16-rod CHF simulation. The local power profile of a typical 6x6 BWR fuel assembly as shown in Figure 17 was modeled by the simulation. Local qualities and mass velocities were calculated via the COBRA Code and are also presented in Figure 17. Regions I, II, III, and IV of the 6x6 fuel assembly were designated to be of primary critical heat flux concern and were simulated closely with the local power distribution of the 16-rod bundle shown in Figure 18. Local qualities and mass velocities for the 16-rod bundle simulation are also provided in Figure 18. The subchannel calculations by COBRA were used to verify the thermal hydraulic simulation of the actual 6x6 fuel assembly using the 16-rod bundle. Comparison of Figures 17 and 18 shows that not only subchannel but also bundle average qualities and mass velocities were reproduced by the 16-rod bundle. This was important since CHF results are established in terms of bundle average mass velocity and quality. Although actual subchannel conditions depend on subchannel mixing, the simulation of the 6x6 fuel bundle by the proposed 4x4 model was insensitive to mixing.

COBRA-II SUBCHANNEL CALCULATIONS
PRESSURE = 1165 psia
AVERAGE HEAT FLUX = 150,460 BTU/HR FT^2

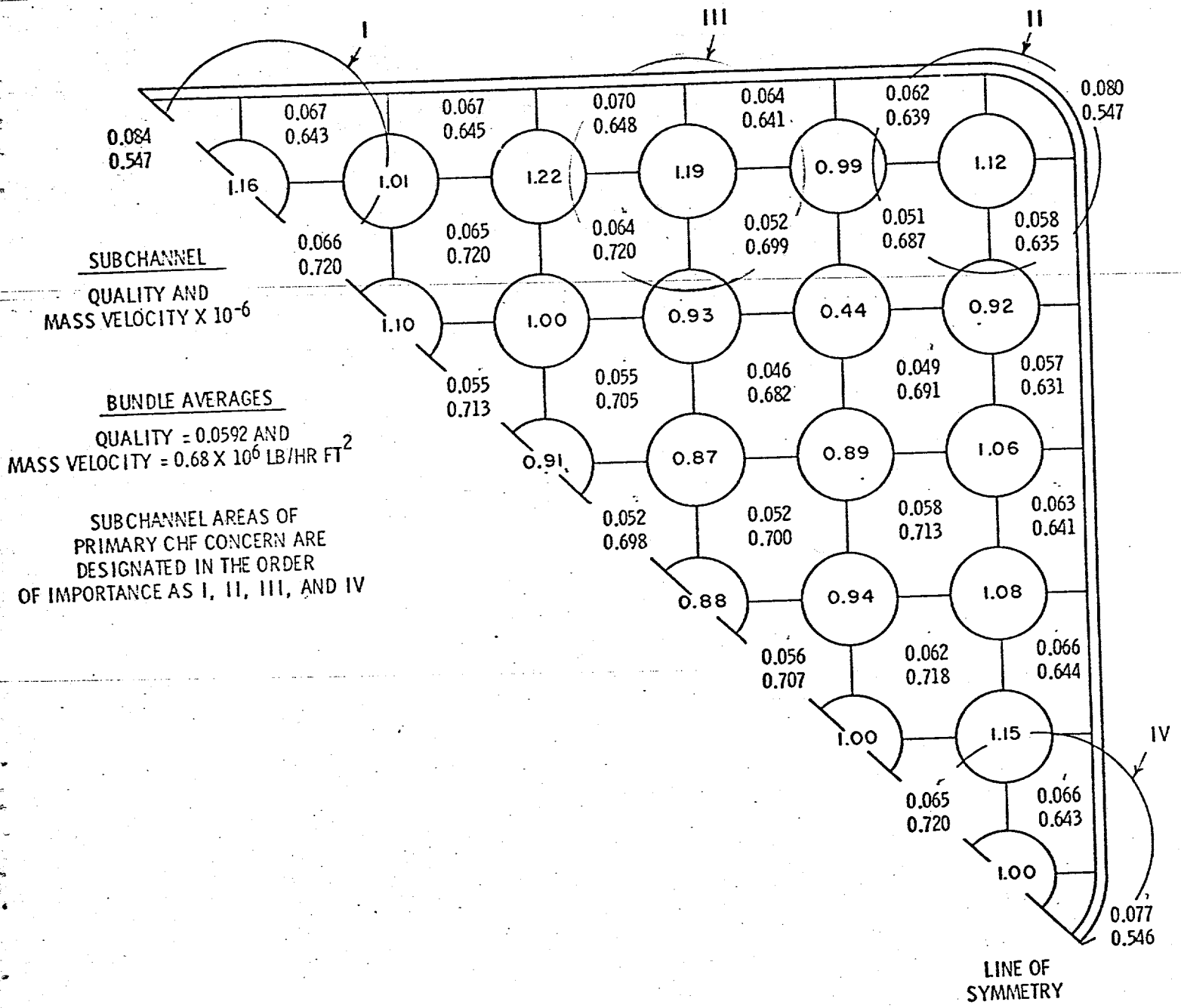

SUBCHANNEL
QUALITY AND
MASS VELOCITY X 10^{-6}

BUNDLE AVERAGES
QUALITY = 0.0592 AND
MASS VELOCITY = 0.68 X 10^6 LB/HR FT^2

SUBCHANNEL AREAS OF
PRIMARY CHF CONCERN ARE
DESIGNATED IN THE ORDER
OF IMPORTANCE AS I, II, III, AND IV

FIGURE 16 MASS VELOCITY AND QUALITY CONDITIONS FOR THE LOCAL POWER DISTRIBUTION OF A BWR FUEL

COBRA-II SUBCHANNEL CALCULATIONS
PRESSURE = 1165 psia
AVERAGE HEAT FLUX = 150,460 BTU/HR FT^2

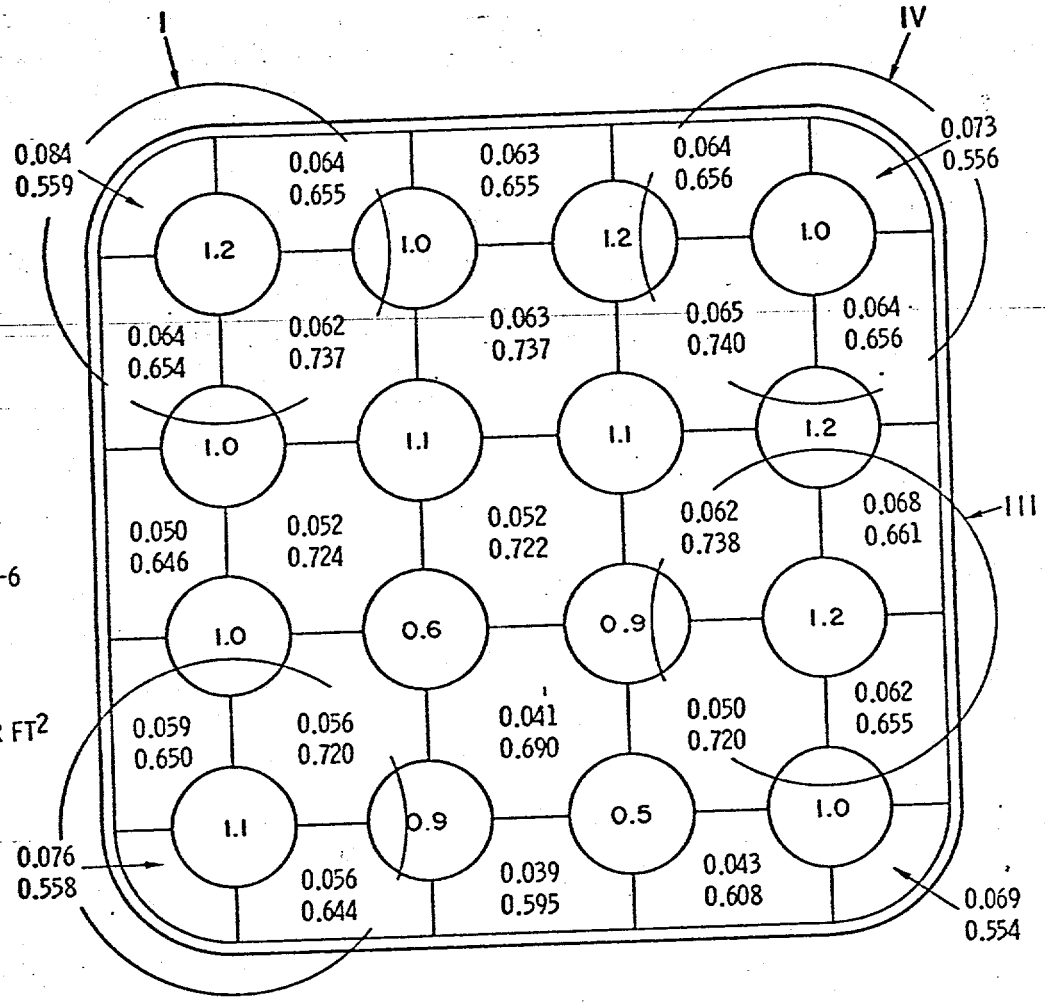

SUBCHANNEL

QUALITY AND
MASS VELOCITY X 10^{-6}

BUNDLE AVERAGES

QUALITY = 0.0578 AND
MASS VELOCITY = 0.68 X 10^6 LB/HR FT^2

SUBCHANNEL AREAS OF
PRIMARY CHF CONCERN ARE
DESIGNATED IN THE ORDER
OF IMPORTANCE AS I, II, III, AND IV

FIGURE 18. MASS VELOCITY AND QUALITY CONDITIONS FOR THE SIMULATED LOCAL POWER DISTRIBUTION OF THE 16 ROD CHF BUNDLE

REFERENCES

1. D.S. Rowe. COBRA-II: A Digital Computer Program for Thermal-Hydraulic Subchannel Analysis of Rod Bundle Nuclear Fuel Elements. BNWL-1229-UC-80, February 1970.

2. E. Janssen et al. Sixteen-Rod Heat Flux Investigation, Steam-Water at 600 to 1250 psia. Two-Phase Flow and Heat Transfer in Rod Bundles. Presented at Winter Annual Meeting of ASME, Los Angeles, California. November 18, 1969, pp. 81-88.

3. S. Israel et al. "Critical Heat Flux Measurements in a 16-Rod Simulation of a BWR Fuel Assembly." Journal of Heat Transfer, August 1969, p. 355.

4. G.A. Sofer & H. Soodak. Nuclear Fuels for Power Reactors. NDEO-1381. Presented at The American Power Conference, Chicago, Illinois, April 23-25, 1968.

5. P. Grillo and V. Marinelli. Pressure Drop Measurements in Isothermal Single-Phase Flow. ANS Winter Meeting, San Francisco, California, November 30 - December 4, 1969, Vol. 12, No. 2, p. 838.